Ion energy distribution function in very high frequency capacitive discharges excited by saw-tooth waveform

Sarveshwar Sharma[1,2], Nishant Sirse[3], Animesh Kuley[4], and Miles M Turner[5]

[1] Basic Theory and Simulation Division, Institute for Plasma Research, Gandhinagar, Gujarat, 382428, India
[2]Homi Bhabha National Institute, Anushaktinagar, Mumbai, Maharashtra, 400094, India
[3]Institute of Science and Research, IPS Academy, Indore, Madhya Pradesh, 452012, India
[4]Department of Physics, Indian Institute of Science, Bangalore, Karnataka, 560012, India
[5]School of Physical Sciences and National Center for Plasma Science and Technology, Dublin City University, Dublin 9, Ireland

Email: nishantsirse@ipsacademy.org

Abstract

Tailoring *ion energy distribution function* (*IEDF*) is vital for advanced plasma processing applications. Capacitively coupled plasma (*CCP*) discharges excited using non-sinusoidal waveform have shown its capability to control *IEDF* through generation of plasma asymmetry and *DC* self-bias. In this paper, we performed a particle-in-cell simulation study to investigate the *IEDF* in a symmetric capacitive discharge excited by saw-tooth like current waveform at a very high frequency (VHF). At a constant driving frequency of 27.12 MHz, the simulation results predict that the ion energy asymmetry in the discharge scales with the discharge current amplitude. A transition from a single narrow ion energy peak to a bi-modal type *IEDF* is observed with an increase in the current density amplitude. Further studies at a constant current density and varying the fundamental excitation frequency shows that the ion energy asymmetry enhances with a reduction in the driving frequency. Increase in the plasma asymmetry and significant *DC* self-bias at lower driving frequency is observed to be one of the principal factors responsible for the observed asymmetry in the ion energy peaks. An investigation of *DC* self-bias and plasma potential confirm that the powered electrode energy peak corresponds to the *DC* self-bias with respect to the plasma potential, and the grounded electrode peak corresponds to the plasma potential. These results suggest that although lower driving frequency is beneficial for generating the discharge asymmetry and large *DC* self-bias, but a narrow low energy *IEDF* is plausible in very high frequency driven *CCP* systems.

1. Introduction

Plasma technology plays a key role in microelectronics device fabrications; particularly in the processes including plasma enhanced chemical vapor deposition (*PECVD*) and plasma etching[1,2]. In such processes, the ion energy distribution function (*IEDF*) on the wafer surface is one of the crucial parameters that drive the surface reactions. A radio frequency (*RF*) capacitively coupled plasma (*CCP*) system, which is a dominant plasma processing tool, mostly generates a broad bi-modal shape energy distribution in which the energy dispersion is defined by the ion transit time (τ_i) and frequency of the applied *RF* field (ω)[3,4]. For the etching applications, as feature sizes are shrinking, one requires a narrow *IEDF* for preventing the surface damage and to increase the selectivity across different materials[5]. In *PECVD* process, controlling the *IEDF* is vital for producing desired microstructures and film properties such as a translation from amorphous to microcrystalline structures[6].

Besides controlling shape of *IEDF*, an independent control of ion energy and ion flux at the substrate is highly desired. In a *CCP* discharge, one way to achieve this is to employ a second frequency either on the same electrode (dual-frequency *CCPs*) or on to the opposite electrode (2-frequency *CCPs*) [7,8]. In such configurations, the ion flux is governed by high frequency, while the low frequency controls the ion energy. Although multiple frequencies operated *CCP* discharges remains a better choice for an independent control of energy and flux, some of the earlier publications reported coupling between 2 frequencies and therefore undesired results are observed[9,10]. Another method for achieving an independent control of ion flux and energy is the Electrical Asymmetry Effect (*EAE*) as proposed by *Heil et al.* [11,12]. In this method, one can generate a *DC* self-bias by changing the phase between a fundamental frequency and its first harmonic in a dual-frequency *CCP* system. In an experimental study by Schulze *et al.*[13], verified that using a variable phase angle between 2 frequencies one could change the average ion energy approximately linearly by keeping the ion flux constant. Using this approach, the simulation results of Donkó *et al.* [14] showed that it is possible to control the shape of *IEDF* at both powered and grounded electrode. In particular, higher moments of the *IEDF* could be varied with a change in the phase angle[15]. However, further studies at different driving frequencies, showed reduced ability of this method to control ion energy ranges at lower driving frequencies due to the secondary electron emissions[16]. Choosing electrodes of dissimilar areas, geometrical asymmetry, and varied materials are other ways for the plasma asymmetry and *DC* self-bias generation[17-20]. A combination of the discharge voltage and driving frequency has been proposed as an alternative approach for an independent control of ion flux and energy[21].

In recent years, generation of electrically asymmetry using a non-sinusoidal waveform has emerged as a promising way to overcome the above challenges[22]. In this method, the use of fundamental and higher harmonics contained in the non-sinusoidal waveform, and phases between them one could generate an asymmetric plasma response even in a geometrically symmetric *CCP*. One of the examples is multi-harmonic waveform in which the plasma density/ion flux at one-electrode increases with the number of harmonics while the average ion energy on the other electrode remains nearly constant[23-26]. Another way to produce asymmetric plasma response is to use the temporally asymmetric waveforms such as saw-tooth like waveforms[27-29]. Such type of asymmetry is known as slope *EAE*. Using such waveforms, a vast disparity in the sheath expansion adjacent to the powered and grounded electrodes generates a strong asymmetry in the ionization rate and thus a flux asymmetry is developed. This effect was further analysed and validated experimentally using Phase Resolved

Optical Emission Spectroscopy (*PROES*)[30]. It was demonstrated that the single frequency generated discharge shows symmetric excitation rate at both electrodes, whereas strong excitation rate asymmetry is observed when the number of harmonics is increased to generate a sawtooth like waveform. It was noticed that by increasing the number of harmonics in the waveform i.e., turning into an ideal sawtooth like waveform further enhances the asymmetry in the discharge[27]. Furthermore, reducing gas pressure have shown that the asymmetry disappears due to a transition from sheath edge ionization to bulk ionization. A study on the different gases revealed that saw-tooth like waveform may cause strong asymmetry depending on the gas used [31].

CCP discharges excited in a very high frequency (VHF) regime have shown several advantages over traditional CCP's excited at 13.56 MHz. In particular, an enhanced plasma density due to lower sheath impedance and reduced ion bombardment energy can be obtained[32,33]. However, VHF plasma excitation generate plasma non-uniformities due to electromagnetic effects[34,35] that limits their advantages for large area processing. Power deposition through multi[36-40], shaped[41-43] electrodes and waveform tailoring[44] showed improvement in the plasma uniformities for VHF plasma excitation. In terms of discharge asymmetry produced by tailored waveform, changing the fundamental driving frequency have shown drastic effect on it. In the case of sawtooth-like voltage waveform, reducing the driving frequency from 54.24 MHz to 1.695 MHz have shown the shifting of ionization peak away from the powered electrodes[27]. Lowering in driving frequency also reduces the ionization rate and thus the density decreases drastically. The combination of above 2 effects makes the discharge asymmetric as driving frequency is reduced. Similar results were observed in the case of saw-tooth like current waveform[29], where a strong asymmetry is observed at 13.56 MHz when compared to 54.24 MHz driving frequency. In addition to the discharge asymmetry, variation in the driving frequency have shown multiple ionization beams that are extended up to the opposite sheath and shown to modify the instantaneous sheath edge positions[29]. The generation of multiple beams, which was also observed experimentally by Berger et al[45], is caused by the self-excitation of higher harmonics. The kinetic mechanism of such self-excitation of higher harmonics was described by Wiczek et al[46,47]. Furthermore, the frequency of the sheath modulation was observed to increase with reducing driving frequency, and therefore proposed as one of the parameters responsible for driving an enhanced plasma density in the discharge at lower fundamental driving frequency[29]. On the other hand, higher beam energy at higher driving frequency was observed, which was due to the increased sheath velocity.

Above studies mostly focused on the electrical asymmetry and the generation of *DC* self-bias in the discharge excited by non-sinusoidal waveforms. On the other hand, there exist very few studies of *IEDF* in such discharge, particularly in VHF regime. One of the simulation studies performed by Schüngel *et al.*[48] demonstrated that by exciting plasma using a tailored waveform consist of 5 harmonics could generate a control over the shape of *IEDF*. In particular, a single peak at low/medium energies within the IEDF could be generated and controlled by adjusting the parameters of the applied voltage waveform. We follow previous studies with the investigation of *IEDF* in the *CCP* discharge using an ideal saw-tooth like current waveform at a very high frequency. In our previous work[29], we focused on the electric field non-linearity and higher harmonics generation in a symmetric *CCP*. In this paper, we extend our previous study[29] and investigate the effect of current density amplitude on the *IEDF* at the powered and grounded electrode in a symmetric *CCP* discharge. A sawtooth like current waveform at a fundamental driving frequency of 27.12 MHz is considered for the present study. Additionally, we also investigate the effect of changing the fundamental driving frequency, from 13.56 MHz to 54.24 MHz, on the shape of *IEDF*. Our simulation results predict ion energy peaks corresponds

to the *DC* self-bias and plasma potential. A narrow *IEDF* is observed at higher fundamental driving frequency.

This research article is organized as follows. The simulation technique that is based on the particle-in-cell/ Monte Carlo collision (PIC/MCC) methods and simulation parameters are described in the section 2. The physical understanding and explanation of the simulation results are presented in the section 3. In section 4, the summary and conclusion are given.

2. Simulation Technique and Parameters

The simulation technique is based on a Particle-in-Cell/Monte Carlo collision (*PIC/MCC*) methods. For the present study, we have used a well-tested and benchmarked 1D3V, electrostatic, self-consistent, *PIC* code[49, 50]. The code has been used extensively in previous studies and details can be found in the literatures[51-63]. As an input, a current waveform is chosen given by the following mathematical expression:

$$J_{rf}(t) = \pm J_0 \sum_{k=1}^{N} \frac{1}{k} \sin(k\omega_{RF} t) \text{ -------- (1)}$$

In the above equation, the positive and negative signs resemble to "sawtooth-down" and "sawtooth-up" waveforms respectively, J_o is the amplitude of current density and ω_{rf} is the fundamental angular *RF*.

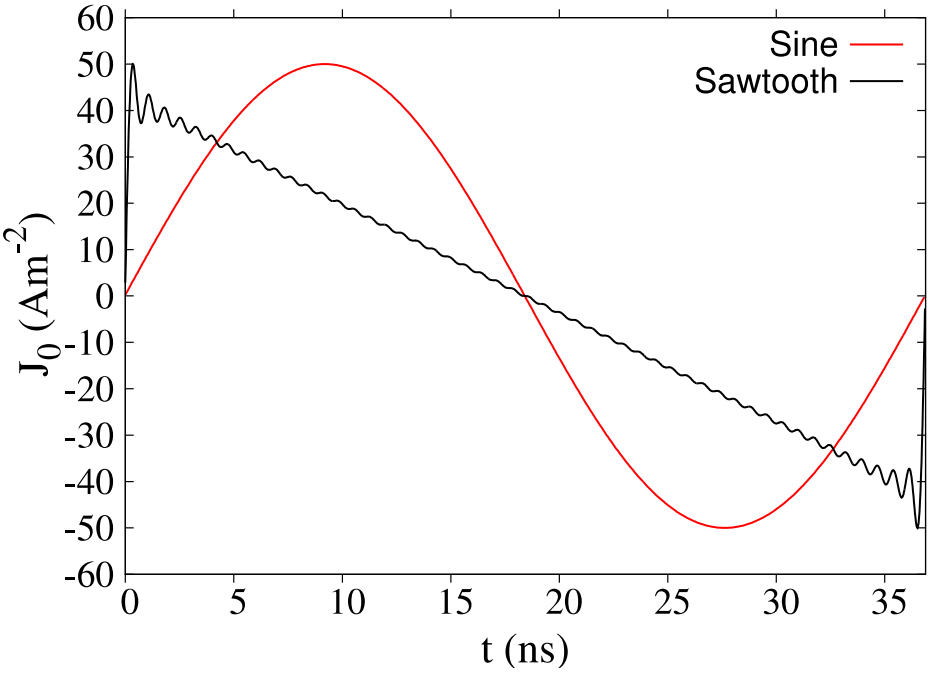

Figure 1: Sinusoidal and sawtooth current waveform at 27.12 MHz fundamental driving frequency and current density amplitude of 50 A/m^2.

An ideal sawtooth waveform is desirable to simulate the asymmetry in the discharge and therefore the waveform should consist of higher number of harmonics. In our case, we have chosen *N=50* harmonics which are distributed in such a way to provide required peak-to-peak current density amplitude for sawtooth current waveform. Using such a large number of harmonics might cause difficulties in order to replicate the simulation results in the experiments due to the matching network issues[64]. However, the current waveform consists of major contribution form the fundamental frequency and other harmonics are below 10% (above N=4) and even lower < 5% (above N=10) for higher harmonics and therefore a comparison with experiments might not be an issue. We also checked the overall trend of simulation results for lower number of harmonics (N=4). It should be emphasized that the choice of current waveform is purely arbitrary as the purpose of this research work is to investigate the *IEDF* for sawtooth waveform and not to replicate or comparison with any specific experiments. One of the advantages for conducting simulation for current waveforms is the validation of the analytical models prediction that is available for the constant current conditions[65,66]. In order to compare with the experiments, though exceptional, a current source can be obtained by implementing an *RF* amplifier or generator with a very high output impedance in comparison to the plasma impedance[67,68]. In this case, one can neglect the additional impedance of the plasma source and consequently current becomes the controlling parameter. The profile of the sawtooth current waveform against sinusoidal waveform is shown in figure 1 for a fundamental driving frequency of 27.12 MHz.

The simulation is performed in argon gas at a fixed gas pressure of 5 mTorr, which is kept constant in the discharge region throughout the simulation. The discharge gap is 6 cm. The sawtooth like current waveform is applied on the electrode at 0 cm and the other electrode at 6 cm is grounded. In the simulation, no external circuit with a capacitor is considered. Therefore, the *DC* self-bias is generated due to the imbalance between electron and ion fluxes arriving at the electrodes caused by the applied waveform. The plasma chemistry considered in the simulation includes several particle-particle reactions such as ion-neutral (elastic, inelastic and charge exchange) and electron-neutral (elastic, inelastic and ionization). The creation of 2 metastable states, Ar^*, and Ar^{**}, is also considered. These two lumped excited states of Ar, *i.e.*, Ar^* (3p54s), 11.6 eV, and Ar^{**} (3p54p), 13.1 eV, in uniform neutral argon gas background is considered with charged particles viz. electrons and ions in the simulation. Important processes like multi-step ionization, metastable pooling, partial de-excitation, super elastic collisions and further de-excitation with their corresponding cross-sections are taken from well-tested source and implemented into the simulation[53, 58, 69].

The stability and accuracy criterion of PIC is achieved by selecting appropriate grid size (Δx) and time step size (Δt) that can resolve the Debye length (λ_{de}) and the electron plasma frequency respectively (f_{pe})[50]. In the present study, the time step (Δt) is of the order of 10^{-11} sec and spatial grid size is of the order of 10^{-4} meter. It is assumed that both the electrodes have infinite dimension and are planar, equal in size i.e. symmetric and parallel to each other. We have also considered that electrodes are perfectly absorbing. The secondary electron emission might play an important role even at a low gas pressure[70,71], however, in the present simulation discharge voltage is low[29] and therefore its effect can be ignored. The neutral gas is uniformly distributed with a fixed temperature of 300^o K throughout the simulation. The temperature of ions is the same as the neutral gas temperature. The number of particles per cell taken here is 100 for all cases. All set of simulations run for more than 5000 *RF* cycles to achieve the steady state profile.

3. Results & Discussions

We first investigate the plasma density in the discharge system by changing the current density amplitude at a fundamental driving frequency of 27.12 MHz. Figure 2 (a) shows the time averaged plasma (ion) density profile for different current density amplitudes ranging from 10 A/m^2 to 125 A/m^2. Corresponding time averaged electron impact ionization rate, $e + Ar \rightarrow 2e + Ar^+$, is plotted in figure 2 (b). For the current set of operating parameters, it is clear from figure 2 (a) that the plasma density at the centre of the discharge is increasing from ~7.8×10^{14} m^{-3} at 10 A/m^2 to ~2.3×10^{16} m^{-3} at 125 A/m^2. On the other hand, the effective electron temperature (T_e) at the centre of the discharge (observed in simulation) decreases from ~2.7 eV at 10 A/m^2 to ~2 eV at 125 A/m^2 *i.e.*, approximately 25% drop in T_e is noticed. The corresponding ionization rate, displayed in figure 2 (b), increases from ~3.0×10^{19} m^{-3}s^{-1} at 10 A/m^2 to ~6.0×10^{20} m^{-3}s^{-1} at 125 A/m^2. Furthermore, due to low gas pressure and longer mean free path the ionization process mainly occur in the plasma bulk. An increase in the ionization rate and hence the plasma density is mostly associated with the enhanced electron power deposition at higher current densities. At a low gas pressure, the electron heating mechanism in RF CCP discharge is overly complex because of nonlinear electron sheath interaction. Various processes such as stochastic, pressure/ambipolar heating have been proposed to elucidate the electron heating mechanism[1,72-76]. It was further demonstrated that even pressure/ambipolar heating mechanism not always dominant at a low gas pressure due to the generation and collisionless transit of energetic electrons beam from near to the sheath edge that greatly attenuates the electron power absorption [77]. The attenuation will be even prominent at a very high frequency because it produces multiple beams of energetic electrons[56-62]. In the present case, the simulation predicts ~20 times increase in the electron heating i.e., from ~250 W/m^3 at 10 A/m^2 to ~5000 W/m^3 at 125 A/m^2. A subsequent increase in the plasma density suggesting that the energy gained by the electrons through interaction with the oscillating sheath dissipates mostly into the ionization processes (single/multi-step). As shown in figure 2 (b) the ionization rate is increasing in proportion to the electron heating in the discharge, which confirm that the ionization is dominant electron energy loss process.

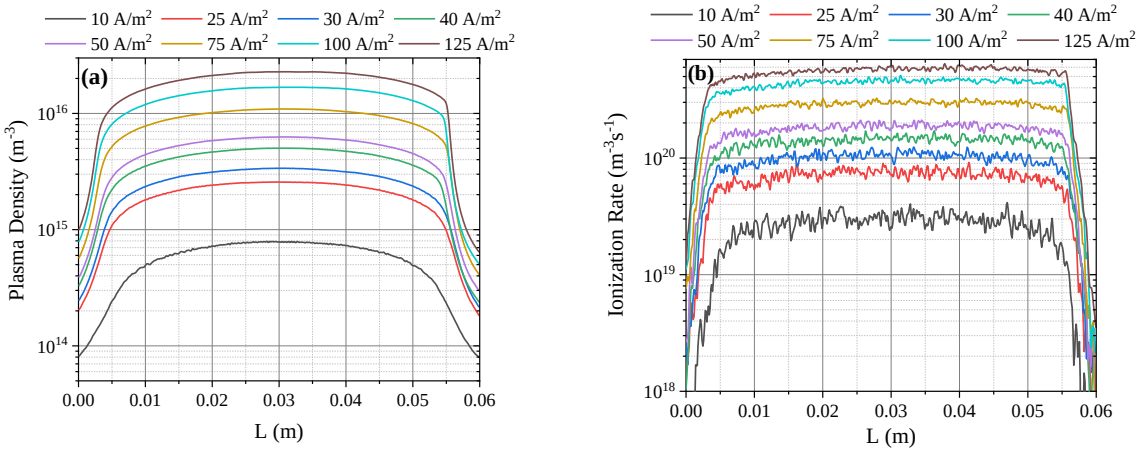

Figure 2**.** The profile of (a) time average plasma density and (b) time average ionization rate for different current densities from 10 A/m^2 to 125 A/m^2 at 27.12 MHz driving frequency.

Further analysis of the plasma density profile shows the generation of discharge asymmetry as the current density increases. Corresponding sheath width, estimated as where the electron sheath edge is at a maximum distance from the electrode and the quasi-neutrality condition breaks down, is nearly the same (approximately 5.5 mm) at both electrodes for a current density of 10 A/m^2. However, as current density amplitude increases to 125 A/m^2 the plasma density profile becomes highly asymmetric. The sheath width at 125 A/m^2 is smaller (~2.7 mm) near to the powered electrode and larger (~4.5 mm) near to the grounded electrode. At higher current density, the asymmetry appears due to the fact that a large *DC* self-bias is generated at the powered electrode. An emergence of *DC* self-bias in a self-consistent manner from the simulation is attributed to the slope asymmetry of saw-tooth like current waveform that generates ionization asymmetry in the discharge[29]. Figure 3 (a) display the time-average potential profile for different current density amplitudes. Corresponding *DC* self-bias at the powered electrode along with the plasma potential versus current density amplitude is shown in figure 3 (b). As shown in figure 3 (a), at 10 A/m^2, the time-averaged potential is nearly the same at both powered and grounded electrode. The potential at the centre of the discharge is ~29 V. As current density amplitude increase, positive *DC* self-bias appears at the powered electrode. As shown in figure 3 (b), both *DC* self-bias and plasma potential scales with current density amplitude reaching to ~130 V and ~200 V at 125 A/m^2 respectively. The difference between plasma potential and *DC* self-bias is also increasing with the current density amplitude.

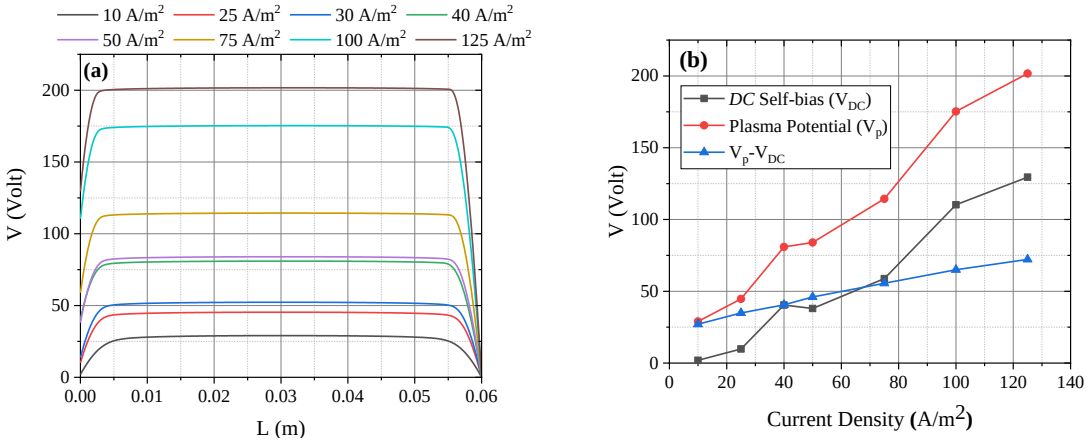

Figure 3. (a) Time-average potential profile and (b) *DC* self-bias at the powered electrode and potential at discharge centre versus current density amplitude. The fundamental frequency of sawtooth waveform is 27.12 MHz.

Figure 4 (a) and 4 (b) shows the normalized *IEDF* at the powered electrode (PE) and grounded electrode (GE) respectively for different current densities from 10 A/m^2 to 125 A/m^2. The fundamental driving frequency is 27.12 MHz. The energy of the different peaks observed in the *IEDF* is also labelled. A clear asymmetry is observed in the ion energy at the powered and grounded electrode. As shown in figure 4 (a) and 4 (b), at 10 A/m^2, the average ion energy is lowest (~26 eV at PE and ~29 eV at GE) and single energy peaks are observed with minimal asymmetry. As the amplitude of current density increases the mean ion energy increases at both PE and GE. However, the ion energy at the GE is consistently higher when compared to the PE. The asymmetry between the energy peaks at the

PE and GE continues to grow with an increase in current density amplitude. At higher current densities, such as 100 A/m^2 and 125 A/m^2, bi-modal energy peaks are observed with a large energy gap between PE and GE. An asymmetry in the energy peaks is attributed to *DC* self-bias at the PE. A self-consistent *DC* self-bias from the simulation is due to an asymmetry in the spatio-temporal ionization rates and electron heating[29]. As shown in figure 3 (b), both plasma potential and *DC* self-bias increase with a rise in current density amplitude and therefore the asymmetry increases. For the present case, the average energy of the PE peaks is consistent with the difference between plasma potential and *DC* self-bias ($V_p - V_{DC}$). On the other hand, the average energy of GE energy peaks corresponds to the plasma potential V_p.

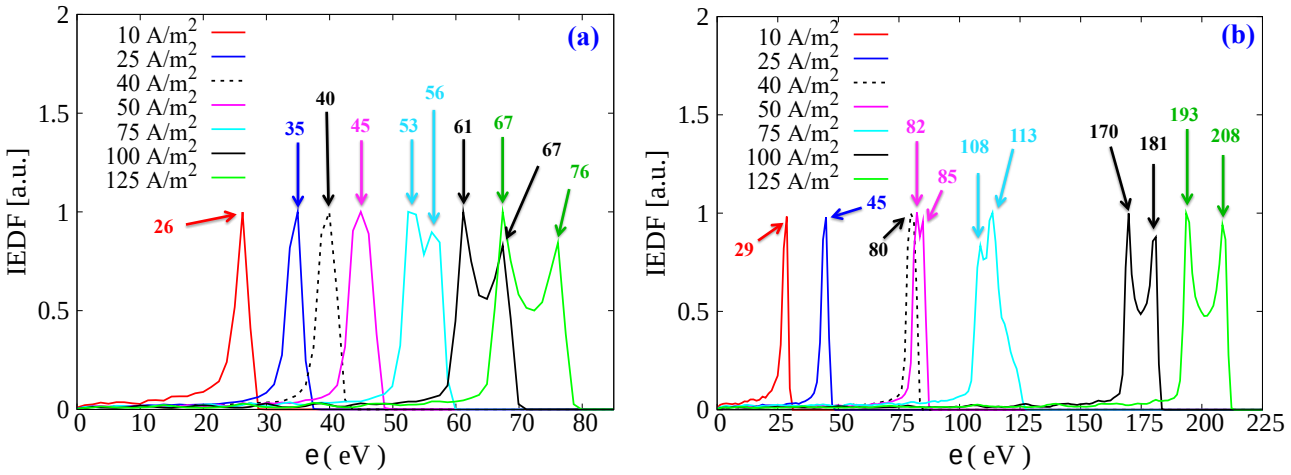

Figure 4. *IEDF* at the a) powered electrode and b) grounded electrode for current density amplitudes from 10 A/m^2 to 125 A/m^2. The fundamental frequency of sawtooth waveform is 27.12 MHz.

An increase in the average ion energy versus current density amplitude is attributed to a change in the sheath width and time averaged sheath voltage. This is due to the fact that ion responds to time average potential. As shown earlier, the plasma is nearly symmetric and sheath width is maximum (~5.5 mm) at 10 A/m^2. A typical ion mean free path for the pressure regime operating here i.e. at 5 mTorr is nearly 0.6 cm. A larger sheath width is responsible for the enhanced ion-neutral collisions. Furthermore, the time averaged potential (figure 3 (b)) at both PE and GE is lowest at 10 A/m^2 and therefore the average ion energy arriving at the electrode decreases. As current density amplitude increases, time averaged potential increases and sheath width decreases, which reduces the ion-neutral collisions within the sheath resulting to a higher average ion energy. On the other hand, the bi-modal behaviour of *IEDF* at higher current densities corresponds to the ion transit time (τ_i) through *RF* sheath. The ion transit time is defined as $\tau_i = 3s_m/v_i \propto V_s^{1/4}/n_s^{1/2}$ where v_i, s_m, V_s, and n_s is the ion velocity in sheath, sheath width, averaged voltage drop across sheath and density at the sheath edge respectively. For a long ion transit time $\tau_i \gg \tau_{rf}$ where τ_{rf} is the *RF* period defined as $\tau_{rf} = 2\pi/\omega_{rf}$. However, for the short ion transit time the condition is $\tau_i \ll \tau_{rf}$[1]. So, the ion energy distribution is broad for short ion transit time case and highly peaked for the long ion transit time case. In the present

case, the ion transit time at the powered electrode for a current density amplitude of 125 A/m^2 is of the order (30-50 ns) of *RF* period (τ_{rf}~37 ns), while at 10 A/m^2 it is ~8 times higher (~300 ns) than *RF* period. Therefore, one will expect a narrow IEDF at lower current density and bimodal at higher current density. For a constant driving frequency/*RF* period, the energy separation *ΔE* between 2 peaks of the bio-modal distribution is proportional to the sheath voltage and inversely proportional to the sheath width i.e. $\Delta E \propto \sqrt{< V_{sh} >}/< s >^3$, where $< V_{sh} >$ is the time-average sheath voltage and $< s >$ is the time-average sheath width. As observed in present work, the sheath width decreases, and averaged sheath voltage increases with a rise in current density amplitude. Therefore, bi-modal peaks with large energy separation are observed at higher current density amplitudes.

The plasma asymmetry is greatly affected by the fundamental driving frequency due to a variation in the *RF* period. Therefore, the role of the driving frequency is crucial in determining the shape of *IEDF*. We investigate this by changing the fundamental driving frequency at a constant current density amplitude. Figure 5 shows the time-average plasma potential [5 (a)], *IEDF* at the powered electrode [5 (b)] and *IEDF* at the grounded electrode [5 (c)] for 3 different driving frequencies: 13.56 MHz, 27.12 MHz and 54.24 MHz at a fixed current density amplitude of 50 A/m^2. The simulations are also performed for lower number of harmonics (N=4) in order to verify the consistency of observed simulation trends. The results are plotted in figure 5 (d) – 5 (f). As shown in figure 5 (a), plasma is highly asymmetric at lowest driving frequency (13.56 MHz) and strong *DC* self-bias (~210 V) is observed at the powered electrode. As the driving frequency increase to 27.12 MHz, significant drop in the *DC* self-bias is observed (~39 V). At 54.24 MHz fundamental driving frequency, the plasma profile is nearly symmetric, and the *DC* self-bias is nearly zero at the powered electrode. For N=4, similar trend is observed i.e., the *DC* self-bias at the PE decreases with a rise in driving frequency expect the absolute value is lower when compared to N=50. The observed behaviour is attributed to the spatio-temporal ionization asymmetry. As observed[29], at lower driving frequency (13.56 MHz), the ionization near to the grounded electrode is higher when compared to powered electrode, whereas, at higher driving frequency (54.24 MHz) the ionization asymmetry reduces drastically.

Further analysis of *IEDF* shape presented in figure 5 (b) and 5 (c), depicts bi-modal distribution at both PE and GE for 13.56 MHz driving frequency along with the strong ion energy asymmetry. The average energy of the PE peak is ~106 eV that corresponds to the *DC* self-bias with respect to the plasma potential, whereas the average energy of the GE peak is ~317 eV that coincide with the time averaged plasma potential. As the driving frequency increase to 27.12 MHz, bi-modal peaks turned into single energy peaks at both PE and GE, and the ion energy asymmetry also decreases i.e., PE peak is observed at 45 eV and averaged ion energy at the GE is at 83.5 eV. Finally, at 54.24 MHz, narrow nearly symmetric energy peaks are observed at PE and GE with ~36 eV and ~ 32 eV ion energy respectively. The conversion into single energy peaks as driving frequency increase is attributed to a drop in the time averaged potential as shown in figure 5 (a). Furthermore, as driving frequency decrease the rf period increase and thus broadening of the energy ion peak is anticipated i.e. $\Delta E \propto < V_{sh} >/\omega$. At 13.56 MHz, strong asymmetry in the ion energy at the PE and GE is due to the generation of large *DC* self-bias (~210 V). Whereas the *DC* self-bias is lowest (~4 V) at 54.24 MHz fundamental driving frequency, which lead to a reduced asymmetry in the average ion energy. As displayed in figure 5 (e) and 5 (f), a transition in the shape of IEDF and ion energy asymmetry versus driving frequency is also true for smaller number of harmonics (N=4). These results support the

validity of overall simulation outcomes and thus an experimental realization could be possible due to less complexity involved in generating sawtooth like waveform with lower number of harmonics.

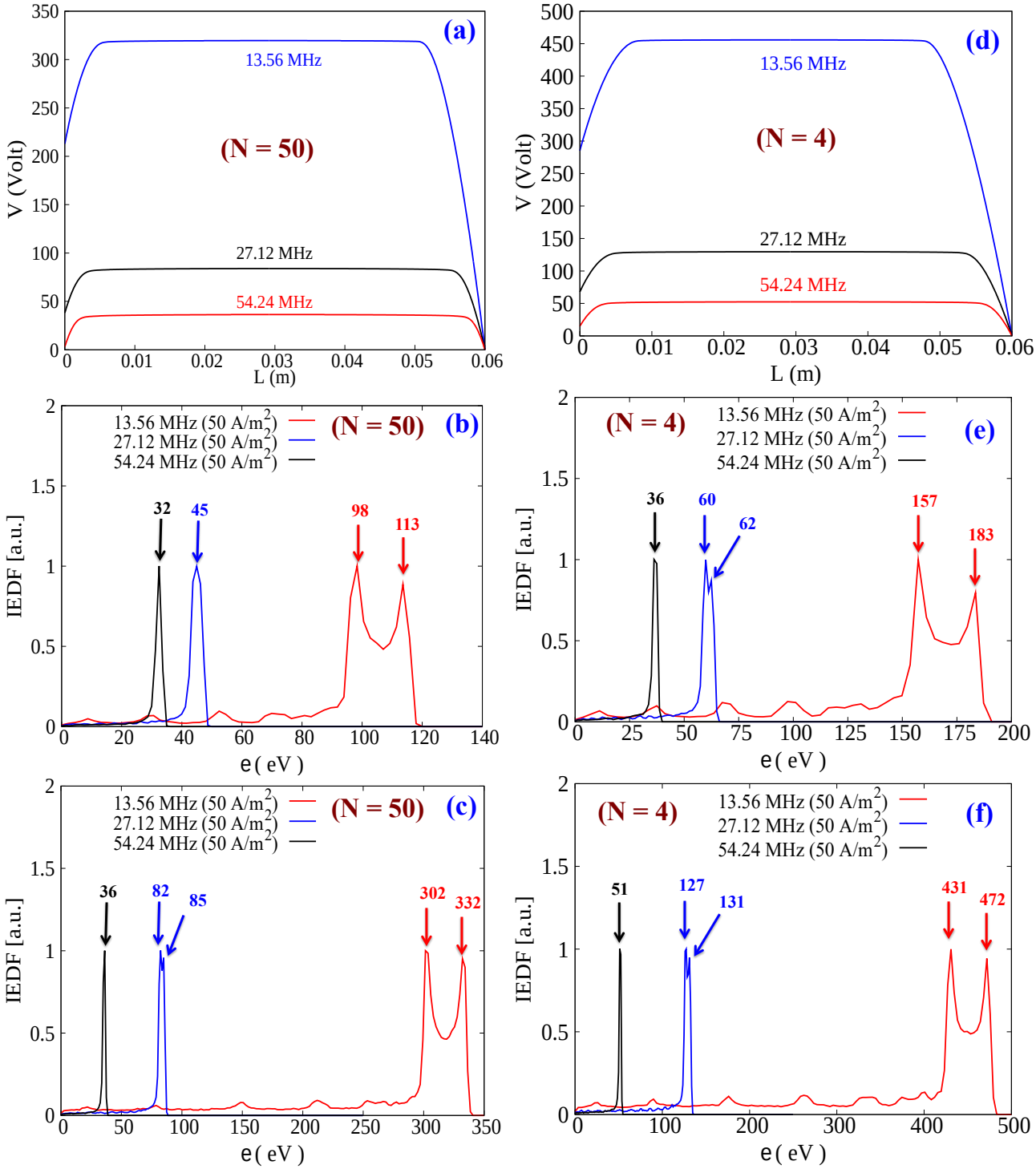

Figure 5. Time-average plasma potential profile ((a) N=50 and (d) N=4), *IEDF* at the powered electrode ((b) N=50 and (e) N=4) and grounded electrode ((c) N=50 and (f) N=4) for 13.56 MHz, 27.12 MHz and 54.24 MHz fundamental frequencies of a sawtooth waveform at 50 A/m^2 current density amplitude.

4. Summary of the work and conclusions

A study of plasma density, *DC* self-bias/plasma potential and *IEDF* is performed using *PIC* simulation is a geometrically symmetric *CCP* discharge excited by a sawtooth like current waveform at a fixed gas pressure of 5 mTorr. For a fundamental driving frequency of 27.12 MHz, the plasma density increases with an increase in the current density amplitude. This is due to an overall increase in the electron heating and ionization rate. The time average plasma potential observes to increase along with the formation of the *DC* self-bias that scales linearly with the current density amplitude. At lower current density amplitude, the plasma is nearly symmetric and the *IEDF* at the powered and grounded electrode shows narrow low energy peak. As current density amplitude increase, bi-modal *IEDF* is observed with a large energy separation between the powered and grounded electrode i.e., the ion energy asymmetry increases. A close observation of *IEDF* suggests that the average ion energies at the PE and grounded electrodes corresponds to the *DC* self-bias and plasma potential. Changing the fundamental driving frequency of sawtooth current waveform leads to a drastic change in the DC self-bias and hence the ion energy asymmetry reduces at higher driving frequencies. A transition in the shape of *IEDF* from bimodal to a narrow single energy peak is observed with increasing driving frequency. For the simulation results it is concluded that although lower fundamental driving frequency of a saw-tooth like waveform is promising for generating discharge/ ion energy asymmetry, but a narrow low energy *IEDF* is mostly possible at a very high frequency due to a reduced rf period and decrease in the averaged sheath voltage.

Acknowledgments

Dr A Kuley is supported by the Board of Research in Nuclear Sciences (BRNS Sanctioned No. 39/14/05/2018-BRNS), Science and Engineering Research Board EMEQ program (SERB Sanctioned No. EEQ/2017/000164), National Supercomputing Mission (NSM) (Ref No: DST/NSM/R&D_HPC_Applications/2021/04) and Infosys Foundation Young Investigator grant.

Conflict of interest

The authors have no conflicts to disclose.

Data Availability

The data that support the findings of this study are available from the corresponding author upon reasonable request.

References:

[1]M Lieberman and A J Lichtenberg, *Principles of Plasma Discharges and Materials Processing* (Wiley, New York, 2005).

[2]P Chabert and N Braithwaite, *Physics of Radio Frequency Plasmas* (Cambridge: Cambridge University Press, 2011).
[3]Theodoros Panagopoulos and Demetre J. Economou, *Journal of Applied Physics* **85,** 3435 (1999).

[4]E Kawamura, V Vahedi, M A Lieberman and C K Birdsall, *Plasma Sources Sci. Technol.* **8,** R45–R64 (1999).

[5]Demetre J. Economou, *Journal of Vacuum Science & Technology* A **31,** 050823 (2013).

[6]G Bugnon, A Feltrin, F Meillaud, J Bailat and C Ballif, *Journal of Applied Physics* **105,** 064507 (2009).

[7]P C Boyle, A R Ellingboe, and M M Turner, *J. Phys. D: Appl. Phys.* **37,** 697 (2004).

[8]T Kitajima, Y Takeo, Z L Petrovic, and T Makabe, *Appl. Phys. Lett.* **77,** 489 (2000).

[9]S K Karkari and A R Ellingboe, *Appl. Phys. Lett.* **88**, 101501 (2006).

[10]T Gans, J Schulze, D O'Connell, U Czarnetzki, R Faulkner, A R Ellingboe, and M M Turner, *Appl. Phys. Lett.* **89,** 261502 (2006).

[11]B G Heil, J Schulze, T Mussenbrock, R P Brinkmann and U Czarnetzki, *IEEE Trans. Plasma Sci.* **36,** 1404 (2008).

[12]B G Heil, U Czarnetzki, R P Brinkmann and T Mussenbrock, *J. Phys. D: Appl. Phys.* **41,** 165202 (2008).

[13]J Schulze, E Schüngel and U Czarnetzki, *J. Phys. D: Appl. Phys.* **42,** 092005 (2009).

[14]Z Donkó, J Schulze, B G Heil and U Czarnetzki, *J. Phys. D: Appl. Phys.* **42,** 025205 (2009).

[15]D J Coumou, D H Clark, T Kummerer, M Hopkins, D Sullivan and S Shannon, *IEEE Trans. Plasma Sci.* **42,** 1880 (2014).

[16]I Korolov, Z Donkó, U Czarnetzki and J Schulze, *J. Phys. D: Appl. Phys.* **45,** 465205 (2012).

[17]J W Coburn and E Kay, *J. Appl. Phys.* **43,** 4965 (1972).
[18]H Köhler, J W Coburn, D E Horne, E Kay and H Keller, *J. Appl. Phys.* **57,** 59 (1985).
[19]M A Lieberman and S E Savas, *J. Vac. Sci. Technol.* A **8,** 1632 (1990).
[20]T Lafleur, P Chabert and J P Booth, *J. Phys. D: Appl. Phys.* **46,** 135201 (2013).
[21]S Sharma, A Sen, N Sirse, M M Turner and A R Ellingboe, *Physics of Plasmas* **25,** 080705 (2018).

[22]T Lafleur, *Plasma Sources Sci. Technol.* **25,** 013001 (2016).

[23]T Lafleur and J P Booth, *J. Phys. D: Appl. Phys.* **45,** 395203 (2012).

[24]P A Delattre, T Lafleur, E V Johnson and J P Booth, *J. Phys. D: Appl. Phys.* **46,** 235201 (2013).

[25]T Lafleur, P A Delattre, E V Johnson and J P Booth J P, *Appl. Phys. Lett.* **101,** 124104 (2012).

[26]T Lafleur, P A Delattre, E V Johnson and J P Booth, *Plasma Phys. Control. Fusion* **55,** 124002 (2013).

[27]B Bruneau, T Novikova, T Lafleur, J P Booth and E V Johnson, *Plasma Sources Sci. Technol.* **24,** 015021 (2015).

[28]B Bruneau, T Novikova, T Lafleur, J P Booth and E V Johnson, *Plasma Sources Sci. Technol.* **23,** 065010 (2014).

[29]S Sharma, N Sirse and M M Turner, *Plasma Sources Sci. Technol.* **29,** 114001 (2020).

[30]B Bruneau, T Novikova, T Lafleur, J P Booth and E V Johnson, *Physical Rev. Lett.* **114,** 125002 (2015).

[31]B Bruneau, T Lafleur, T Gans, D O'Connell, A Greb, I Korolov, A Derzsi, Z Donkó, S Brandt, E Schüngel, J Schulze, P Diomede, D J Economou, S Longo, E Johnson and J-P Booth, *Plasma Sources Sci. Technol.* **25,** 01LT02 (2016).

[32] A. A. Howling, J. L. Dorier, C. Hollenstein, U. Kroll and F. Finger , *J. Vac. Sci. Technol. A* **10**, 1080 (1992).

[33]M. Surendra and D. B. Graves, *Appl. Phys. Lett.* **59**, 2091 (1991).

[34]M. A. Lieberman, J. P. Booth, P. Chabert, J. M. Rax, and M. M. Turner, *Plasma Sources Sci. Technol.* **11**, 283 (2002).

[35]A. Perret, P. Chabert, J. Jolly and J.-P. Booth, *Appl. Phys. Lett.* **86(1)**, 021501 (2005).

[36]C. Harvey, **N. Sirse**, C. Gaman and A. R. Ellingboe, *Physics of Plasmas* **27,** 22844 (2020).

[37]N. Sirse, C. Harvey, C. Gaman and A. R. Ellingboe, *J. Phys. D: Appl. Phys.* **53,** 335203 (2020).

[38]A. R. Ellingboe: "*Plasma Source*," US Pat. 7,342,361 B2 (2008).

[39]E. Monaghan, T. Michna, C. Gaman, D. O'Farrel, K. Ryan, D. Adley, T. S. Perova, B. Drews, M. Jaskot, and A. R. Ellingboe, *Thin Solid Films* **519** (20), 6884 (2011).

[40]K. S. Kim, N. Sirse, K. H. Kim, A. R. Ellingboe, K. N. Kim, and G. Y. Yeom, *J. Phys. D. Appl. Phys.* **49(39)**, 395201 (2016).

[41]H Schmidt, L Sansonnens, A A Howling, C Hollenstein, M Elyaakoubi and J P M Schmitt, *J. Phys. D: Appl. Phys.* **95,** 4559 (2004).

[42]L. Sansonnens and J. Schmitt, *Appl. Phys. Lett.* **82(2)**, 182, (2003).

[43]P. Chabert, J.-L. Raimbault, J.-M. Rax and A. Perret, *Phys. Plasmas* **11**, 4081 (2004).

[44]E Schüngel, S Mohr, J Schulze and U Czarnetzki, *Appl. Phys. Lett.* **106,** 054108 (2015).

[45]B Berger, K You, H-C Lee, T Mussenbrock, P Awakowicz and J Schulze, *Plasma Sources Sci. Technol.* **27,** 12LT02 (2018)

[46]Sebastian Wilczek, Jan Trieschmann, Denis Eremin, Ralf Peter Brinkmann, Julian Schulze, Edmund Schuengel, Aranka Derzsi, Ihor Korolov, Peter Hartmann, Zoltán Donkó, *and* Thomas Mussenbrock, *Physics of Plasmas* **23**, 063514 (2016)

[47]S Wilczek, J Schulze, R P Brinkmann, Z Donkó, J Trieschmann, and T Mussenbrock, *Journal of Applied Physics* **127**, 181101 (2020).

[48]E Schüngel, Z Donkó, P Hartmann, A Derzsi, I Korolov and J Schulze, *Plasma Sources Sci. Technol.* **24,** 045013 (2015).

[49]R W Hockney and J W Eastwood, *Computer simulation using particles* (Adam Hilger, Bristol, 1988).

[50]C K Birdsall, *Plasma physics via computer simulation* (Adam Hilger, Bristol, 1991).

[51]M M Turner, A W Hutchinson, R A Doyle and M B Hopkins, *Phys. Rev. Lett.* **76,** 2069 (1996).

[52]P C Boyle, A R Ellingboe and M M Turner, *Plasma Sources Sci. Technol.* **13,** 493 (2004).

[53]L Lauro-Taroni, M M Turner and N St J Braithwaite, *J. Phys. D: Appl. Phys.* **37,** 2216 (2004).

[54]M M Turner, *Plasma Sources Sci. Technol.* **22,** 055001 (2013).

[55]J Conway, S Kechkar, N O Connor, C Gaman, M M Turner and S Daniels, *Plasma Sources Sci. Technol.* **22,** 045004 (2013).

[56]S Sharma, N Sirse, P K Kaw, M M Turner and A R Ellingboe, *Phys. Plasmas* **23,** 110701 (2016).

[57]S Sharma, A Sen, N Sirse, M M Turner and A R Ellingboe, *Physics of Plasmas* **25,** 080705 (2018).

[58]S Sharma, N Sirse, M M Turner and A R Ellingboe, *Physics of Plasmas* **25,** 063501 (2018).

[59]Sarveshwar Sharma, N Sirse, A Sen, J S Wu, and M M Turner, *J. Phys. D: Appl. Phys.* **52,** 365201 (2019).

[60]S Sharma, N Sirse, A Sen, M M Turner and A R Ellingboe, *Physics of Plasmas* **26,** 103508 (2019).

[61]S Sharma, N Sirse, A Kuley and M M Turner, *Plasma Sources Sci. and Technol.* **29,** 045003 (2020).

[62]S Sharma, N Sirse, A Kuley, A Sen and M M Turner, *J. Phys. D: Appl. Phys.* **54,** 055205 (2020).

[63]S Sharma, S K Mishra, P K Kaw and M M Turner, *Physics of Plasmas* **23,** 013509 (2017).

[64]Junkang Wang, Sebastien Dine, Jean-Paul Booth, and Erik V. Johnson, *J. Vac. Sci. Technol. A* **37**, 021303 (2019).

[65]M M Turner and P Chabert, *Appl. Phys. Lett.* **104,** 164102 (2014).

[66]M M Turner and P Chabert, *J. Phys. D: Appl. Phys.* **50,** 23LT02 (2017).

[67]V A Godyak, *Soviet Radio Frequency Discharge Research* (Falls Church, VA: Delphic, 1986).

[68]W D Qiu, K J Bowers and C K Birdsall, *Plasma Sources Sci. Technol.* **12,** 57 (2003).

[69]R Shahid and Mark J Kushner, *J. Appl. Phys.* **82,** 2805 (1997).

[70]B Horv´ath, M Daksha, I Korolov, A Derzsi and J Schulze, Plasma Sources Sci. Technol. **26**, 124001 (2017).

[71]B Horv´ath, J Schulze, Z Donk´o and A Derzsi, *J. Phys. D: Appl. Phys.* **51**, 355204 (2018).

[72] M M Turner, *Phys. Rev. Lett.* **75**, 1312 (1995).

[73]S Sharma and M M Turner *Plasma Sources Sci. Technol.* **22,** 035014 (2013).

[74]S. Sharma, "*Investigation of ion and electron kinetic phenomena in capacitively coupled radio-frequency plasma sheaths: A simulation study*," Ph.D. thesis (Dublin City University, Ireland, 2013).

[75]S Sharma and M M Turner *J. Phys. D: Appl. Phys.* **46,** 285203 (2013).

[76] J Schulze, Z Donkó, T Lafleur, S Wilczek, and R P Brinkmann, *Plasma Sources Sci. Technol.* **27**, 055010 (2018).

[77] M Vass , S Wilczek, T Lafleur, R P Brinkmann, Z Donkó and J Schulze, *Plasma Sources Sci. Technol.* **29,** 085014 (2020).